Journal of Electronics and Electrical Engineering
https://ojs.wiserpub.com/index.php/JEEE

Research Article

Enhancing Low-Voltage Ride-Through Capability of Wind Turbine Based Double-Fed Induction Generator Using ANFIS Controller and Crowbar Circuit

Ashraf K. Abdelaal[1*], Mahmoud A. M. Algoul[2], Attia A. El-Fergany[3]

[1]Department of Electric Power and Machine, Faculty of Technology, Suez University, Suez, 43512, Egypt
[2]Department of Electric Power and Machine, Faculty of Engineering, College of Engineering Technology (Houn) Libya
[3]Department of Electric Power and Machine, Faculty of Engineering, Zagazig University, Zagazig, 44519, Egypt
E-mail: Ashraf.Abdelaal@ind.suezuni.edu.eg

Received: 14 March 2025; **Revised:** 17 April 2025; **Accepted:** 7 May 2025

Abstract: The main target of this paper is to increase the low-voltage ride-through (LVRT) of the Doubly fed induction generator (DFIG) driven by wind turbine. Two steps are suggested to achieve this goal, firstly, by inserting a crowbar circuit (CB) into rotor circuit, in case of voltage dip (VD), to protect it from excessive current and excessive voltage that could result from the transient flux produced by the VD. It is worth to note that simulation results proved that if no CB circuit is used, the system may be vulnerable to instability. Next, an ANFIS-controller is proposed to control both the rotor side converter (RSC) and the grid side converter (GSC). The GSC is controlled such that the suggested controller will enhance LVRT by injecting the needed system reactive power. While the RSC controller regulates the electromagnetic torque, the GSC controller control both the real power and reactive power delivered to the system during normal operating conditions beside with it keeps the value of the dc link voltage fixed. From the results, it is clear that the hybrid ANFIS and CB circuit are capable of sustaining the DFIG stability and provide an improved LVRT responses in challenging operating conditions and within the acceptable criterions.

Keywords: double fed induction generator, low voltage ride through, wind turbine, field oriented control, crowbar circuit, adaptive neuro fuzzy inference system

1. Introduction

Double fed induction generator (DFIG) is the most superior generator used in wind turbine (WT) power generation, since its power electronics converter has 25-30% of the generator capacity [1]. However, DFIG is responsive to system faults as its stator coils are directly joined to the electrical system [2]. Since power systems are vulnerable to contingencies, there are reported problems caused by the integration of DFIG to the power systems [2]. In addition, the dynamic response of DFIG is governed by non-linear variables, the operation and controlling of DFIG under fault conditions is a real challenge nonetheless the system fault happened away from the generator. If a high size WT is suddenly stopped generation system stability will be affected [3]. Therefore, power system operator necessitates certain rules or requirements concerning the insertion of any renewable power sources into power systems grid and any new renewable power sources, to be connected to the grid, must obey these grid codes [4], [5].

DOI: https://doi.org/10.37256/jeee.4120256745

1.1 *Basic information about the LVRT problem*

Based on the above-mentioned rules, DFIG must remain working during voltage fluctuations for a specific duration and deliver reactive power (QP) through the voltage fluctuations. This process is termed LVRT which is explained by a relation that links the voltage with time by a curve that state the minimum allowable voltage sag and its time duration [6]-[8]. Although there are many codes to deal with LVRT, Figure 1 describes the general LVRT capability curve for system requirements for DFIG connection [7]. As seen from this figure, network codes necessitate a DFIG has to survive voltage dip (VD) even if it lasts for long period, after this duration the DFIG could be disjointed from the grid to bypass its harm [9]. Accordingly, the DFIG must fulfil the LVRT standards to confirm the behavior of the system and participate in controlling the voltage via harsh network disturbance. Consequently, it is necessary to insert protection circuits and/or use new control techniques to enhance LVRT capability.

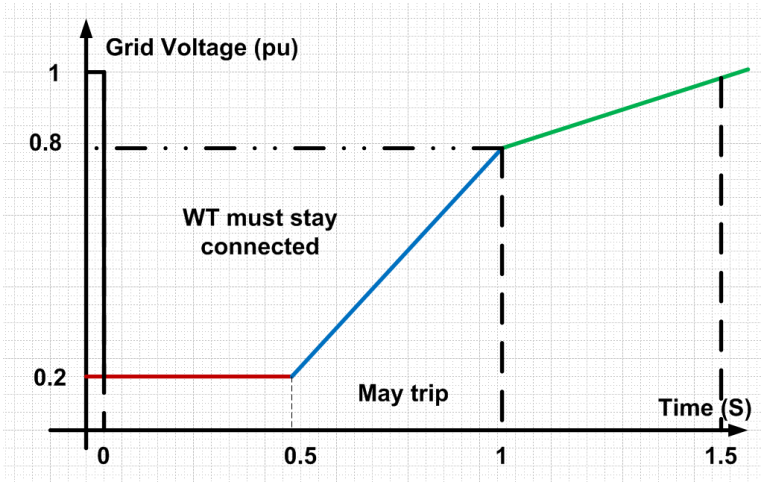

Figure 1. The general LVRT capability curve for system requirements

The normal operation of DFIG is explained in details in [10], which will be helpful to understand how to operate DFIG in efficient way at a specified operating point. When a grid containing DFIG is subjected to voltage dips, since DFIG is mainly inductive circuit, there will be a transient current and voltage component that are fixed with respect to the stator (i.e., they are DC with reference to the stator windings). Both components are dependent on the time, type, and the magnitude of the sag, as a result it will strongly affect the LVRT response to any voltage changes. Since the relative speed, between the resulting transient flux and the rotor conductors, is the rotor speed (not the slip velocity as in normal operation). As a result, the induced emf in the rotor conductors will be high and is reliant on the magnitude of the VD and the occurring moment [9].

The overvoltage in the rotor circuit would result in the initiation of the guard circuit and DFIG interruption. This possibly causes abrupt fall of huge amount of energy, and therefore increasing the effects of the problem. The recognition of the starting time of the voltage change is crucial for the enhancement of the DFIG. Oliveira [11] stated that it is crucial to consider enough details about the voltage change type and grid connections. Considering simple models would produce a severe false estimation of the influence of the voltage sags on the DFIG. Oliveira showed that the magnitude of the VD affects significantly the DC link voltage (DCLV) and stated that there is necessity to include the dip details. Power systems grids necessitate that wind turbines (WTs) should remain in operation without separating them from the system under voltage dips for definite duration. Usually this duration is 0.15 s for low voltage levels of 0 till 0.1 pu [12]. Concurrent, power systems grids dictate that DFIG should deliver the needed QP to the grid to restore voltage profile [13], [14]. Related grid codes are suggested for LVRT in many countries around the world [5], [15].

There are many methods to deal with the LVRT issue, the first category is created by power electronics devices like crowbars (CB), static VAR compensator (SVC), dynamic voltage restorer (DVR), unified power flow controller (UPFC),

braking chopper, and static synchronous compensator (STATCOM). The second depends on energy storage systems in connection with power electronics switches. The third category is based on advanced control techniques for example pitch angle control [16] predictive control [17], [18], and vector control methods [19], [20]. A comprehensive review on various LVRT methods could be found in [5], [21]-[24].

1.2 *LVRT scenario*

As mentioned before, when a fault happens in a power system, there will be an abrupt change in the value of the voltage of the DFIG. This will lead to unexpected rises in stator and rotor (SAR) current. This will affect the DCLV and perhaps destroy the rotor side converter (RSC). To guard the RSC, a CB circuit is implanted in the rotor circuit of the generator at the instant of the VD to isolate and protect the RSC. A rule for CB firing when the rotor current (ROTCNT) will be equal to or higher than 2 pu [25]. A CB circuit combined with a DC-chopper circuit are used in [26] to improve LVRT. A CB circuit with an Energy Storage System (ESS) was applied in [27] to increase LVRT competence. DVR is used with super magnetic energy-storage to overcome LVRT during voltage sags [28]. Another device is used to enhance LVRT is the DVR and it is used in [29] to compensate for any voltage shortage, where fuzzy logic controller (FLC) was applied to tune the compensation. Another approach is to use ANN to regulate the DVR to enhance the LVRT ability of the grid is suggested in [30]. DVR beside with reactive fault current limiter (FCL) are used [31] to get effective LVRT technique for DFIG.

1.3 *Power electronics-based methods*

SVC is common in power systems and is adopted to control voltage and QP. In Ref. [32], SVC is used to improve LVRT with the help of FLC. The STATCOM is used to increase LVRT of the generator by supporting the voltage at the connection point during VD [33]. A metaheuristic optimization is used to tune STATCOM to increase the LVRT competency of the generator during VD [34]. While Ding [35] used a FLC beside with STATCOM to increase the LVRT. Another FLC is adopted to tune STATCOM to improve the competences of the LVRT of the generator [36].

In Ref. [37], a power electronics bridge circuit, which is similar to a single phase uncontrolled rectifier that is controlled by electronic switch in cascade with a diode. The diode is connected with a low shunt inductance that is in series with too low resistance. This circuit is used to bound the current throughout faults situations. A hybrid scheme is introduced, which consists of a FCL and a DC-DC converter or chopper circuit (CC) as reported in ref. [38]. A double protection scheme is used, first is a CB circuit to protect the RSC, while the other is a CC to guard the DC link (DCL) [39]. Makolo [40] suggested method consists of a capacitance in cascade with an inductance and the combination is linked in shunt to a resistance. This scheme is joined to the RSC through inductance and resistance branch. The unified power quality conditioner is applied to compensate for any voltage dips to enhance LVRT [41].

1.4 *Energy storage-based methods*

ESS is used with other devices to supply power during system faults. Tait [12] concluded that ESS schemes should be the preferred option to enhance LVFRT of big-size wind turbines. An ESS is used with DVR to correct and restore the voltage profile [42]. Both the superconductor FCL and super magnetic energy-storage were adopted to enhance the LVRT by specifying their optimum positions using metaheuristic optimization [43].

All the previous devices are expensive and will add additional costs to the higher costs of DFIG WT system, which will make the total costs high, so another view is to avoid adding any hardware devices and use control theory to enhance LVRT. One important feature for any controller is the necessity for the generator to supply QP during the LVRT period [44]. Jiateng [45] showed that in unbalanced fault conditions there would be an ac flux component in the synchronously rotating frame that will affect the operation of the PI control and he suggested a technique based on model predictive control, which will enhance LVRT response. Also, Refs. [46], [47] used predictive control without any CB to improve LVRT.

1.5 *Vector control-based methods*

Other control techniques used vector control (VC) to enhance LVRT, for example Kumar [48] made a comparison between four methods used for controlling DFIG, namely VC, direct torque control, direct power control, and the derivative of these methods. He concluded that the choice of specific regulation method depends on the requirements. VC is used to control DFIG to decouple active and reactive power [49]. Yuan in Ref. [50] showed that the DFIG regulated by VC is comparable to a voltage source that can be applied to enhance the QP transfer of the generator. Chowdhury [51] used nonlinear control theory to regulate both the RSC and GSC at same time to increase LVRT ability. Mostafa [52] used Bonobo optimizer to obtain the optimal magnitudes of the inserted rotor voltage angle into the generator. These values are applied to get the maximum QP for assisting the system voltage throughout abnormal circumstances.

Mansoor [53] presents a method to deal with LVRT where the GSC has a parallel transformer to inject current to preserve the ROTCNT within acceptable levels. A simple protection scheme is introduced by Kasem [54], where the scheme is a resistor joined in cascade to the rotor coils. However, this is not recommended since it will rise the rotor voltage to high value in case of short circuit which may threaten the RSC.

1.6 *Advanced control-based methods*

Hiremath [55] suggested a new version of sliding mode regulator to improve LVRT during abnormal voltage conditions. Sabbir [56] proposed a supportive control technique contains resistor to limit current and added signal to the current in the control method to enhance LVRT. Mosayyebi [57] stated that ambiguities and parameter changes will produce negative impacts on the response of the LVRT techniques. To cope with these issues, he recommended using automatically noise elimination techniques such as auto disturbance rejection control.

Rafiee [58] concentrated on the transient voltage regulation to enhance LVRT. Herzog [59] stated that rotor velocity is very crucial to LVRT since it affects the slip of the machine; therefore, it will affect the machine dynamic during abnormal conditions. Also He stated that Power system parameters strongly affect the response of the DFIG to LVRT [59]. The most important parameter is the power system impedance at the point of common coupling. The impedance of the grid governs the amount of voltage deviation while supplying QP to the grid. In addition, the X/R ratio is another important parameter [59].

1.7 *Paper main contributions and structure*

The main contributions of the current work are summarized as follows:

1) To improve the LVRT, it suggests a hybrid design that incorporates both an ANFIS and a CB circuit. The suggested scheme protects the rotor of the DFIG during VD, in addition to support the system voltage during any voltage dips.

2) Formulation, analysis, and investigation of the stator flux's transient component's effects on the DFIG variables are implemented.

3) Using Simulink/MATLAB environment, the suggested scheme is created completely, and the results are investigated.

This paper is organized as follow: This Section 1 introduces a detailed review of the different methods that are used to enhance the LVRT capabilities. The second Section announces notes about the methods to alleviate the LVRT impacts, which include the CB circuit rule, describe the dynamic voltage restore rule in increasing the LVRT competency and the working principle of the DC-DC converter to increase the LVRT. The model of the DFIG is given in Section 3, while the transient effect of the VD on the model of the DFIG is presented in Section 4. Section 5 describes the proposed ANFIS controller. The recommended scheme is specified and outlined in Section 6, and the simulation results and analyses are given in Section 7. The concluding remarks are given in the last section.

2. Methods used to alleviate the LVRT effects

The main goal of the LVRT is to keep the DFIG working during fault, to protect the rotor circuit from voltage rise during fault, and to help in restoring network voltage to its nominal values. The existing methods to perform these tasks are CB circuit, DVR, and DC to DC converter. The operation principle of each device will be explained in the next lines.

2.1 *Crowbar circuit*

The CB is the most dominant LVRT protection scheme that is adopted to guard the RSC of DFIG from excessive currents or voltages. A CB circuit consists of a resistance connected in series to a three-phase uncontrolled rectifier that is controlled by a series IGBT switch. As the CB circuit is inserted, the DFIG is converted to a squirrel cage induction generator and its stator windings absorb a high quantity of QP from the grid, which may deteriorate the terminal voltage dynamics. Disconnecting the CB will promote the RSC to supply QP to the system at once to speed up the system voltage restorer. It should be noted that enough time is required for the CB to guarantee that the transient flux is decreased to a required value to help the RSC to restore the generator control [60]. Consequently, the insertion period of the CB circuit has to be selected cautiously to enhance the transient behavior of DFIG. The other vital issue, which affects the performance of the CB, is the resistance value. In order to choose the magnitude of R_{crow}, there are two contradicting constraints, the first one is that the value of R_{crow} has to be high enough to bound the ROTCNT to protect the rotor conductors. But a high value of the CB resistance causes high voltage in the rotor and DCL, that could damage the rotor windings. On the other hand, a low value of CB resistance results in a high ROTCNT and torque pulsations [60]. Thus, a suitable magnitude of the CB resistance should be carefully chosen. Different values of R_{crow} are examined for different values of voltage fluctuations, and a good value of R_{crow} may be found in [61].

$$R_{\text{crow}} = \omega_r \sqrt{L_s L_{\sigma s} - 2L_{\sigma}^2} \tag{1}$$

where $L_s = L_{\sigma s} + L_m$, $L_{\sigma} = L_{\sigma s} + L_{\sigma r}$, $L_{\sigma s}$, and $L_{\sigma r}$ are the leakage inductance of SAR coils, and L_m is the mutual inductance. As seen from the equations, the value of R_{crow} depends on the DFIG parameters.

2.2 *Dynamical voltage restorer (DVR)*

DVR is a voltage source inverter (VSI) with LC filter and the VSI is joined to the system through a transformer [62]. DVR senses for any fluctuations in the voltage then compensates these fluctuations by injecting voltage into the network to restore the voltage to its rated level. The magnitude and the angle of the compensated voltages can be controlled, so this permits to the regulation of both RP and QP between the DVR and system [42]. So the main target of the DVR is preserve the voltage profile constant during any grid faults [63]. In normal grid operation, the DVR is inactive and no power exchange with the system. During abnormal voltage sags, the DVR is activated and begins to compensate for the voltage sags. There are two forms of DVR, the first one uses energy storage systems to correct and restore the voltage profile [42]. The other one has no energy storage systems and draws current from the system to correct the voltage profile.

2.3 *Chopper or DC-DC converter (CC)*

A CC is controlled by fast switch connected in cascade with a resistor to decrease the high voltage of the DCL capacitor throughout system voltage fluctuations. The relation of the DCLV is stated as:

$$C \frac{\mathrm{d}v_{dc}}{\mathrm{d}t} = i_{GSC} - i_{RSC} \tag{2}$$

where v_{dc} is the DCLV, i_{GSC} is the GSC current, and i_{RSC} is the RSC current. The stored energy of the capacitance is the difference between the power exchange between GSC and RSG, neglecting converter losses and can be expressed as [64]:

$$\frac{1}{2}C\,\frac{\mathrm{d}V_{dc}^2}{\mathrm{d}t^2} = P_{GSC} - P_{RSC} \tag{3}$$

where P_{GSC} is the GSC power, and P_{RSC} is the RSC power. This equation shows that during voltage fluctuations of the DCLV could be decreased by wasting the additional energy to the resistance of the CC. The duty ratio (D) of the chopper switch could be calculated from the following equation [64]:

$$D = \frac{R_{\text{chopper}}}{V_{dc}^2} \cdot (P_{GSC} - P_{RSC}) \tag{4}$$

where R_{chopper} is the chopper resistance.

3. The dynamical model of the DFIG in vector control

In regular operation, the power system can be represented as three phase-balanced voltages source of constant amplitude and frequency, which can be expressed as a space phasor. The armature and rotor circuit relations of the generator in a reference frame (RefF) that is revolving the synchronous speed, ω_s are given by the following space vector equations which can be further represented in a synchronously revolving dq RefF and separating d- and q-axis parts, the dq-axis voltage equations for DFIG are given in [9]

$$\vec{v}_s = R_s\,\vec{i}_s + p\,\vec{\lambda}_s + j\omega_s\vec{\lambda}_s \quad \rightarrow \quad \begin{cases} v_{ds} = R_s i_{ds} + p\lambda_{ds} - \omega_s\lambda_{qs} \\ v_{qs} = R_s i_{qs} + p\lambda_{qs} + \omega_s\lambda_{ds} \end{cases} \tag{5}$$

$$\vec{v}_r = R_r\,\vec{i}_r + p\,\vec{\lambda}_r + j(\omega_s - \omega_r)\vec{\lambda}_r \quad \rightarrow \quad \begin{cases} v_{dr} = R_r i_{dr} + p\lambda_{dr} - (\omega_s - \omega_r)\lambda_{qr} \\ v_{qr} = R_r i_{qr} + p\lambda_{qr} + (\omega_s - \omega_r)\lambda_{dr} \end{cases} \tag{6}$$

$$\vec{\lambda}_s = L_s\,\vec{i}_s + L_m\,\vec{i}_r \tag{7}$$

$$\vec{\lambda}_r = L_r\,\vec{i}_r + L_m\,\vec{i}_s \tag{8}$$

where $\vec{v}_s$, $\vec{v}_r$ are SAR voltage space vectors (V). v_{ds}, v_{dr}, v_{qs} and v_{qr} are the SAR d- and q-axis voltage (V) defined as: $\vec{v}_s = v_{ds} + jv_{qs}$ and $\vec{v}_r = v_{dr} + jv_{qr}$. $\vec{i}_s$, $\vec{i}_r$ are the SAR current space vectors (A). i_{ds}, i_{dr}, i_{qs} and i_{qr} are the SAR d- and q axis current (A) defined as: $\vec{i}_s = i_{ds} + ji_{qs}$ and $\vec{i}_r = i_{dr} + ji_{qr}$. $\vec{\lambda}_s$, $\vec{\lambda}_r$ are the SAR space flux linkage vectors (Wb). λ_{ds}, $\lambda_{dr}, \lambda_{qs}$ and λ_{qr} are the SAR d- and q axis fluxes (Wb) defined as: $\vec{\lambda}_{\mathbf{s}} = \lambda_{ds} + j\lambda_{qs}$ and $\vec{\lambda}_r = \lambda_{dr} + j\lambda_{qr}$. R_s, and R_r are the coil **resistances** of SAR (Ω). ω_s is the RefF synchronous speed (rad/s). ω_r is the electric angular velocity of the rotor (rad/s). p is the differential operator ($p = \frac{\mathrm{d}}{\mathrm{d}t}$).

$j\omega_s \overrightarrow{\lambda}_s$ and $j(\omega_s - \omega_r)\overrightarrow{\lambda}_r$ in Equations (5) and (6) represent the rotational voltages, that are induced in SAR because of the relative velocity between of the synchronously rotating RefF and both SAR. All constants and variables of the rotor, such as R_r, L_{lr}, $\overrightarrow{i}_r$ and $\overrightarrow{\lambda}_r$, are referred to the stator. The synchronous speed ω_s is $2\pi f_s$, and the slip speed between the rotor and the synchronously reference frame is given by:

$$\omega_{sl} = \omega_s - \omega_r \tag{9}$$

The angle θ_s that is necessary to transfer from stator frame into the synchronously frame and can be computed from

$$\theta_s(t) = \int_0^t \omega_s(t)\mathrm{d}t + \theta_0 \tag{10}$$

where θ_0 defines the initial angular position.

The position angle of the rotor θ_r is referred to the stator frame. The slip angle that separates the stator voltage (SV) space vector and the rotor is

$$\theta_{sl} = \theta_s - \theta_r \tag{11}$$

The *dq-axis* RefF revolves at velocity ω_s, that is related to θ by

$$\omega_s = \frac{\mathrm{d}\theta_s}{\mathrm{d}t} \tag{12}$$

The flux linkages dq-components are calculated from:

$$\begin{cases} \lambda_{ds} = L_s i_{ds} + L_m i_{dr} \\ \lambda_{qs} = L_s i_{qs} + L_m i_{qr} \\ \lambda_{dr} = L_r i_{dr} + L_m i_{ds} \\ \lambda_{qr} = L_r i_{qr} + L_m i_{qs} \end{cases} \tag{13}$$

The motion equation that relates the electromagnetic torque (EMT), T_e with the mechanical torque (MT), T_m and is given by:

$$J\frac{\mathrm{d}\omega_m}{\mathrm{d}t} = T_e - T_m \tag{14}$$

The electrical torque can be represented in stator, rotor and *dq*-axis flux linkages and currents. Therefore, many equations for the torque exist and the frequently used equations are described by

$$\begin{cases} T_e = \frac{3P}{2} Re\left(j\overrightarrow{\lambda}_s \overrightarrow{i}^*_s\right) = -\frac{3P}{2} Re\left(j\overrightarrow{\lambda}_r \overrightarrow{i}^*_r\right) \\ T_e = \frac{3P}{2}\left(i_{qs}\lambda_{ds} - i_{ds}\lambda_{qs}\right) \\ T_e = \frac{3P}{2} L_m \left(i_{qs}i_{dr} - i_{ds}i_{qr}\right) \\ T_e = \frac{3P}{2}\frac{L_m}{L_r}\left(i_{qs}\lambda_{dr} - i_{ds}\lambda_{qr}\right) \end{cases} \tag{15}$$

where J is the inertia constant of the rotor in kg $\cdot$ m^2, P defines pole pairs, ω_m is rotor mechanical velocity, and $\omega_m = \omega_r/P$ in rad/s

Equations (5) to (15) depict the dq-model of the machine in RefF revolves at the synchronous velocity. Equation (15) is crucial for the model of the generator in vector control, as aligning the SV or flux, or rotor flux in the d axis direction, a model for the DFIG can be produced. For example, by aligning the stator flux (SF) vector in the d-axis direction, then $\lambda_s = \lambda_{ds}$ and $\lambda_{qs} = 0$. Similarly, if one uses the rotor flux in d axis $\lambda_r = \lambda_{dr}$ and $\lambda_{qr} = 0$, and this is called rotor flux-oriented control. If one uses the SV (that is known as the systems voltage and is easily measurable) instead of the flux, then it is called SV oriented control. It's important to note that in normal operation and by using Equation (5), there is a very small difference between the oriented control and SV oriented control $\overrightarrow{v}_s = R_s \overrightarrow{i}_s + \omega_s \overrightarrow{\lambda}_s$, if we neglect the stator resistance voltage drop then

$$\overrightarrow{v}_s = j\omega_s \overrightarrow{\lambda}_s \tag{16}$$

which is direct relation between SV and SF. If one uses stator field-oriented control then Equations (5) and (6) are represented in the following form, which represent the model of the stator field model of the DFIG.

$$\begin{cases} \frac{d\lambda_{ds}}{dt} = v_{ds} - R_s i_{ds} \\ \lambda_{qs} = 0 = L_s i_{qs} + L_m i_{qr} \rightarrow i_{qr} = -\frac{L_s}{L_m} i_{qs} \\ \frac{d\lambda_{dr}}{dt} = v_{dr} - R_r i_{dr} + (\omega_s - \omega_r)\lambda_{qr} \\ \frac{d\lambda_{qr}}{dt} = v_{qr} - R_r i_{qr} - (\omega_s - \omega_r)\lambda_{dr} \\ T_e = \frac{3P}{2} i_{qs}\lambda_{ds} \rightarrow i_{qs} = \frac{2}{3P}\frac{T_e}{\lambda_{ds}} \end{cases} \tag{17}$$

4. Effect of voltage fluctuations on DFIG

If the SV before fault is $\widehat{V}_s$ and the SV after fault is $\widehat{V}_{sf} = (1 - Dip)\widehat{V}_s$, then difference between the pre- and post- SV is $\left(\widehat{V}_s - \widehat{V}_{sf}\right) = Dip \times \widehat{V}_s$ (where Dip is per unit voltage change).

$$\overrightarrow{v}^s_s(t < 0) = \widehat{V}_s\, e^{j\omega_s t} \tag{18}$$

$$\overrightarrow{v}^s_s(t \geq 0) = (1 - Dip)\widehat{V}_s\ \ e^{j\omega_s t} \tag{19}$$

Grid code rules usually stipulate that voltage drop lasts for a time interval in the order of 1 to 2 ms. The pre-fault SV equation of the DFIG is:

$$\frac{\mathrm{d}}{\mathrm{d}t}\ \overrightarrow{\lambda}^{s}_{s}\ +\ \frac{R_s}{L_s}(\overrightarrow{\lambda}^{s}_{s}-L_m\ \overrightarrow{i}^{s}_{r})=\ \overrightarrow{v}^{s}_{s} \tag{20}$$

Let the rotor circuit is opened (the effect of the ROTCNT will be shown at the next step),

$$\frac{\mathrm{d}}{\mathrm{d}t}\ \overrightarrow{\lambda}^{s}_{s}\ +\ \frac{R_s}{L_s}\overrightarrow{\lambda}^{s}_{s}=\ \overrightarrow{v}^{s}_{s} \tag{21}$$

Then the resulting equation is a linear differential equation of order 1; the solution of this equation is simple and has two components: the natural or transient solution and the particular or forced solution. The forced flux component magnitude is an ac component that has a space vector revolving at the synchronous speed and is proportional to the system voltage. It can be calculated as:

$$\overrightarrow{\lambda}^{s}_{sf}=\ \frac{\widehat{V}_{sf}}{j\omega_s}\ e^{j\omega_s t}=\ \frac{(1-Dip)*\widehat{V}_s}{j\omega_s}e^{j\omega_s t} \tag{22}$$

The other part of the SF is the transient flux resulted from the change in the voltage magnitude. Its initial value is $\overrightarrow{\lambda}^{s}_{sno}$ and it exponentially decreasing. The transient flux depends on the initial conditions of the DFIG. It will occur even if the voltage drops to zero at the DFIG terminals. The initial value of the natural flux $\overrightarrow{\lambda}_{sno}$ is calculated at t = 0 by remembering that the SF should have the same value instantaneously before and after the voltage drop.

$$\overrightarrow{\lambda}_{sno}=\ \frac{\widehat{V}_{sf}}{j\omega_s}=Dip*\frac{\widehat{V}_s}{j\ \omega_s} \tag{23}$$

So the magnitude is of the natural SF component is $\overrightarrow{\lambda}_{sno}\ \ e^{-t/\tau_s}$. This competent is fixed to stator (not rotating)

$$\overrightarrow{\lambda}_{sn}=Dip\ \ \frac{\widehat{V}_s}{j\ \omega_s}\ \ \ e^{-t/\tau_s} \tag{24}$$

The total SF is the addition of the two components $\overrightarrow{\lambda}^{s}_{s}=\ \frac{\widehat{V}_{sf}}{j\omega_s}\ e^{j\omega_s t}+\overrightarrow{\lambda}_{sno}\ \ e^{-t/\tau_s}$, and after substitution becomes $\overrightarrow{\lambda}^{s}_{s}(t\geq 0)=(1-Dip)\ \frac{\widehat{V}_s}{j\ \omega_s}\ e^{j\omega_s t}+Dip\frac{\widehat{V}_s}{j\ \omega_s}\ \ e^{-\frac{t}{\tau_s}}$, which leads to the final form as described in (25).

$$\overrightarrow{\lambda}^{s}_{s}(t\geq 0)=\ \frac{\widehat{V}_s}{j\ \omega_s}\ [(1-Dip)*e^{j\omega_s t}+Dip*e^{-\frac{t}{\tau_s}}\ ] \tag{25}$$

The SF has two components. The first is the forced flux, it varies sinusoidally as the source, and the other is a DC stationary and decaying component for the natural flux component. The SC can be calculated as

$$\overrightarrow{i}^{s}_{s}(t\geq 0)=\frac{\widehat{V}_s}{j\ \omega_s L_s}\left[(1-Dip)*e^{j\omega_s t}+Dip*e^{-\frac{t}{\tau_s}}\right] \tag{26}$$

The distinction between the SAR fluxes has a low value because of the leakage inductances. The rotor flux can be computed as $\overrightarrow{\lambda}^r_r = \frac{L_m}{L_s}\ \overrightarrow{\lambda}^r_s + \ \sigma\, L_r\, \overrightarrow{i}^r_r$

Where $\sigma\ \left(=\ 1-\ L_m^2/L_sL_r\ \right)$ is the coefficient of leakage. As assumed before the rotor circuit is opened and knowing that the rotor is moving at ω_m relative to the SF so the rotor flux space vector can be calculated as

$$\overrightarrow{\lambda}^r_r = \frac{L_m}{L_s}\ \frac{\widehat{V}_s}{j\ \omega_s}\ \left[(1-Dip)*e^{js\omega_s t} + Dip*e^{-(\frac{t}{\tau_s}+j\ \omega_m t)}\ \right] \tag{27}$$

This rotor flux induces an emf in the rotor circuit, $\overrightarrow{v}^r_{r-ind}$ given by $\overrightarrow{v}^r_{r-ind} = \frac{d}{dt}\overrightarrow{\lambda}^r_r = \ \overrightarrow{v}^r_{rf-ind} + \ \ \overrightarrow{v}^r_{rn-ind}$.

The first component of the rotor induced voltage resulted from the forced flux component. This voltage component is analogous to the induced voltage during standard operations. Its value is proportional both the relative speed between the flux and rotor conductors and also it depends on the SF magnitude:

$$\overrightarrow{v}^r_{rf-ind} = \ \frac{L_m}{L_s}\ \frac{\widehat{V}_{sf}}{j\omega_s}\ \frac{d}{dt}\ \left[e^{j(\omega_s-\omega_m)t}\right] = \ \frac{L_m}{L_s}\frac{\widehat{V}_{sf}}{j\omega_s} js\omega_s\ \ e^{j\omega_r t} = \frac{L_m}{L_s}(1-Dip)s\ \widehat{V}_s\ e^{j\omega_r t} \tag{28}$$

This induced forced voltage is quite small for two reasons the first reason is that the system voltage during voltage dip $\widehat{V}_{sf} = (1-Dip)\widehat{V}_s$ is low and the second reason is the value of the slip is low too. The other induced rotor voltage component is induced by the stator natural flux. It can be calculated as:

$$\overrightarrow{v}^r_{rn-ind} = \frac{\mathrm{d}}{\mathrm{d}t}\ \overrightarrow{\lambda}^r_{rn-ind} = \frac{L_m}{L_s}\frac{Dip*\widehat{V}_s}{j\omega_s}\frac{\mathrm{d}}{\mathrm{d}t}[e^{-\left(\ \frac{1}{\tau_s}\ +j\omega_m\right)t}\ ]$$

$$= -\frac{L_m}{L_s}\ \ \frac{Dip*\widehat{V}_s}{j\omega_s} * \left(\frac{1}{\tau_s}\ + j\omega_m\right) e^{-(\ \frac{1}{\tau_s}\ +j\omega_m)t} \tag{29}$$

The term $\frac{1}{\tau_s}$ is small since $\frac{1}{\tau_s} \ll j\omega_m$, it could be neglecting and $\omega_m = (1-s)\omega_s$, so

$$\overrightarrow{v}^r_{rn-ind} = -\frac{L_m}{L_s}\ \ \frac{Dip*\widehat{V}_s}{j\omega_s} * j\omega_s(1-s) * e^{-\left(\ \frac{1}{\tau_s}\ +j\omega_m\right)t}$$

$$= -\frac{L_m}{L_s}\ \ Dip*\widehat{V}_s*(1-s)*e^{-(\ \frac{1}{\tau_s}\ +j\omega_m)t} \tag{30}$$

Rotor induced emf is the addition of the two components which could be written in the final form as

$$\overrightarrow{v}^r_{r-ind} = \ \frac{L_m}{L_s}[\ s\ (1-Dip)\ \ e^{j\omega_r t} - (1-s)\ Dip*e^{-j\omega_m t}e^{-\frac{t}{\tau_s}}\ ]\widehat{V}_s \tag{31}$$

The two rotor voltage components in the last equation are dissimilar in nature. The first one is resulted from the post-fault system voltage and its magnitude is small as explained earlier. Its frequency is very low, in the range of a few hertz, since it is identical to the distinction between the synchronous velocity and the rotor velocity. The second term is the

natural voltage resulted from the transient flux. Its amplitude is high since it is multiplied by the factor (*1-s*), and it has a frequency determined by the rotor shaft velocity, ω_m.

To consider the influence of the ROTCNT on the rotor voltage, it will affect it by two folds [9]. Firstly, it will speed up the decrease of the natural flux. The other is it will influence on the rotor voltage due to voltage drop.

5. Adaptive neuro-fuzzy inference system architecture

ANFIS is an artificial intelligent method that combines of two soft computing techniques of Takagi-Sugeno fuzzy inference system and artificial neural network (ANN). ANFIS has the self-learning capability to approximate nonlinear systems. Using ANFIS, one can use only the system input/output numerical data for modelling without knowing the exact predetermined model structure. ANFIS is used only for Takagi-Sugeno type fuzzy system inference and for one output only.

ANFIS architecture composed of five layers. Each layer has a specific function [65] .

- Layer number 1 performs the fuzzification process as in fuzzy logic, since it receives the crisp input data and assign to each input data the suitable degree of the membership function.
- Layer number 2 is in charge of creating the firing powers for the rules, and it is specified as rule layer.
- Layer number 3 normalizes the calculated firing powers, by dividing every value for the entire firing power.
- Layer number 4 the normalized values from layer 3 are replaced by their crisp values using defuzzification process.
- Layer number 5 this layer has only one node that computes the whole sum of all the incoming signals from the preceding node to get the output value [66].

FL is selectd in this paper because it is a superior choice for managing system uncertainty. The Fuzzy controller could be implemented as a set of IF-THEN rules. The univese of discourse is divided into number of languistic variables (LV) , each LV has specific range with certain shape. In the current work, 10 LV are used with triangle shape as shown in Figure 2a. The ANFIS controller is a combination of fuzzy logic and neural networks. A range of inputs are used to train the neural network, and the inputs dictate the network's typical output. The output of the neural network is input into fuzzy logic after training, which generates the membership functions and IF THEN rules. MATLAB is used to carry out this procedure. The ANN learning is used to train both the input and output of a PID-controller. Back propagation ANN is used in this work for learning.The ANFIS controller is established to enhance the LVRT of the DFIG. In ANFIS, the user cannot modify the number of ANFIS' layers, but can select the shape of the membership functions used which is shown in Figure 2 in addition to the ANFIS model structure.

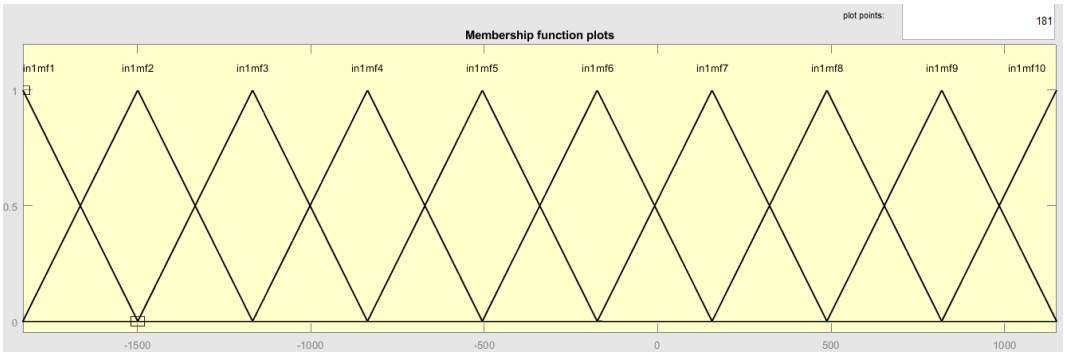

(a)

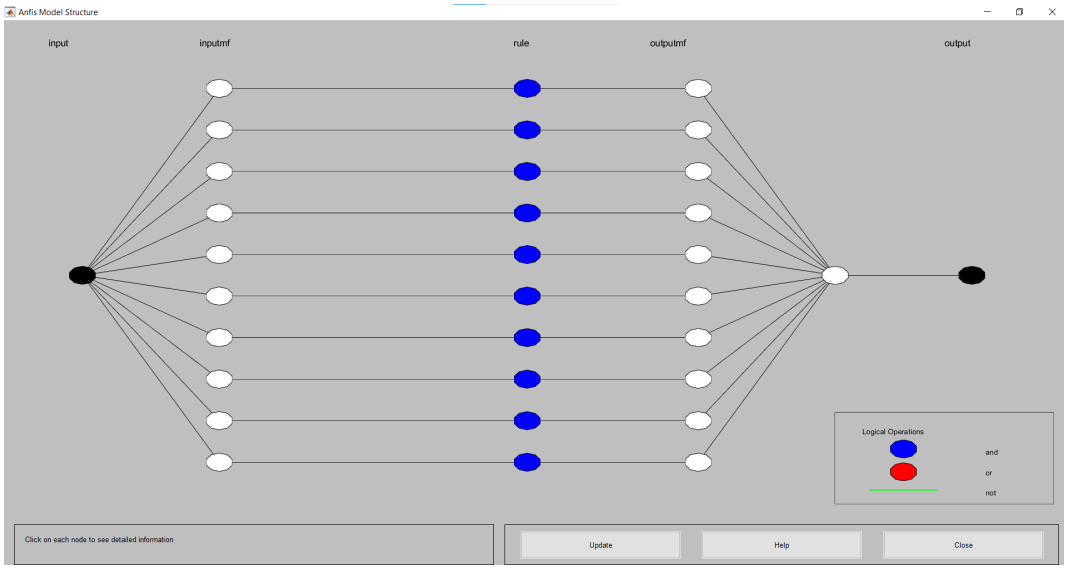

(b)

Figure 2. Fuzzy structure: (a) The used membership functions. (b) the ANFIS model structure

6. Proposed control technique

The key task of this paper is to increase the LVRT capability of the DFIG. The task can be realized in two parallel stages. The first stage by inserting the CB resistor in the rotor circuit when fault takes place in the grid then controlling both the RSC and GSC during normal operation and modify the control starategy to control both controllers during system fualts. The compelete system is revealed in Figure 3a,b, which displays the WT based DFIG with a crow bar circuit in the rotor cicuit.

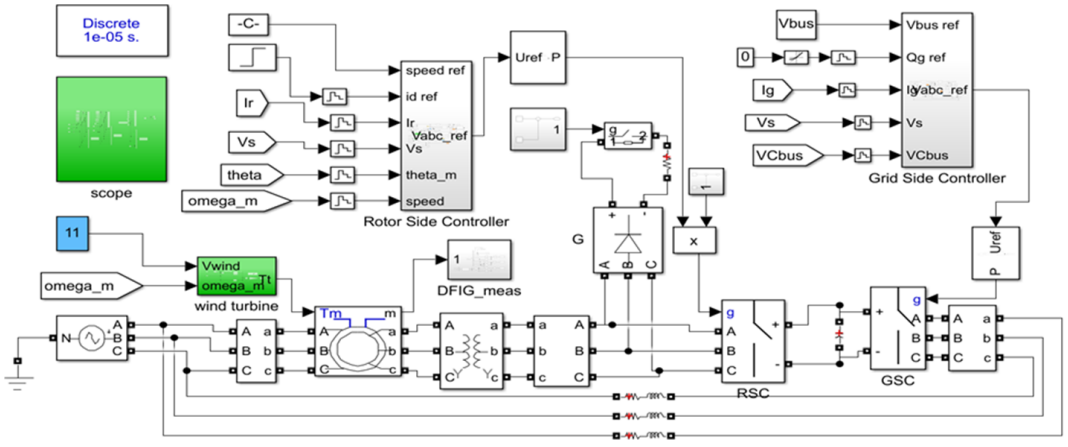

(a) Detailed scheme

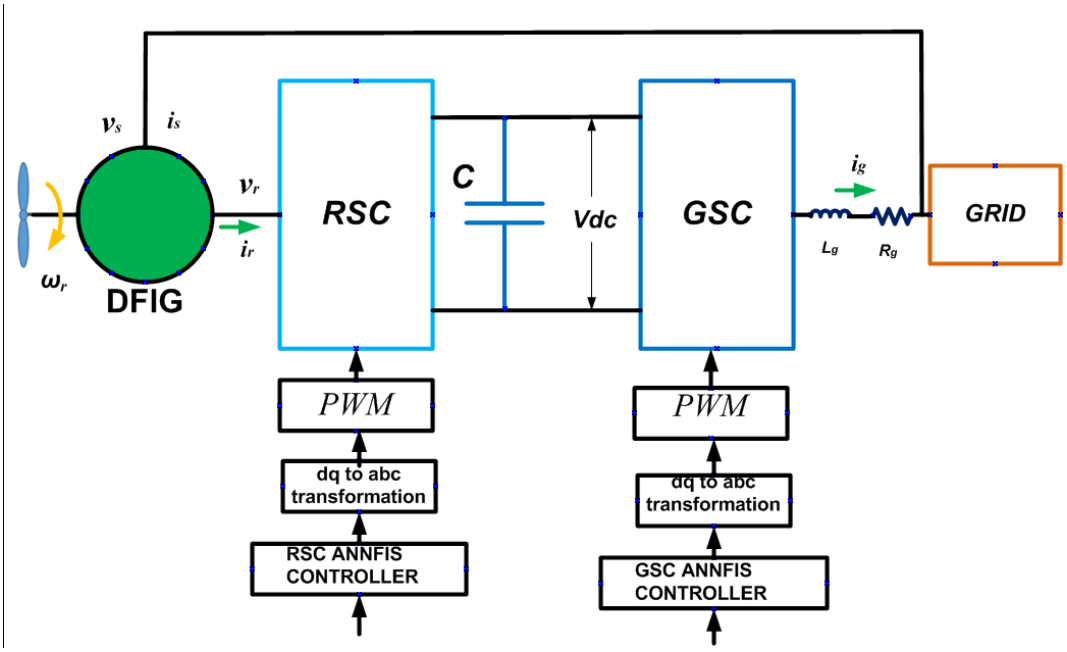

(b) Simplified block diagram

Figure 3. The proposed scheme block diagram

A CB circuit consists is shown in Figure 3 and has a resistance connected in series to a three-phase uncontrolled rectifier that is controlled by a series IGBT switch. The control law to switch on the IGBT switch is that once the ROTCNT or voltage exceed specified limits.

6.1 *RSC control*

The suggested RSC controller used for regulating the dq parts of the current in the RSC is clarified in Figure 4.

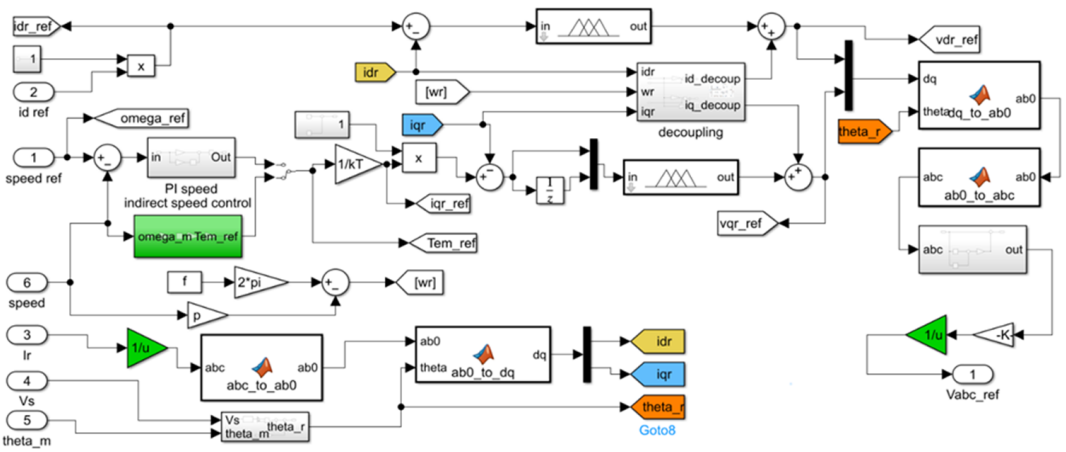

Figure 4. The RSC of the proposed technique

6.2 *GSC control*

The connection diagram of CSC controller is illustrated in Figure 5.

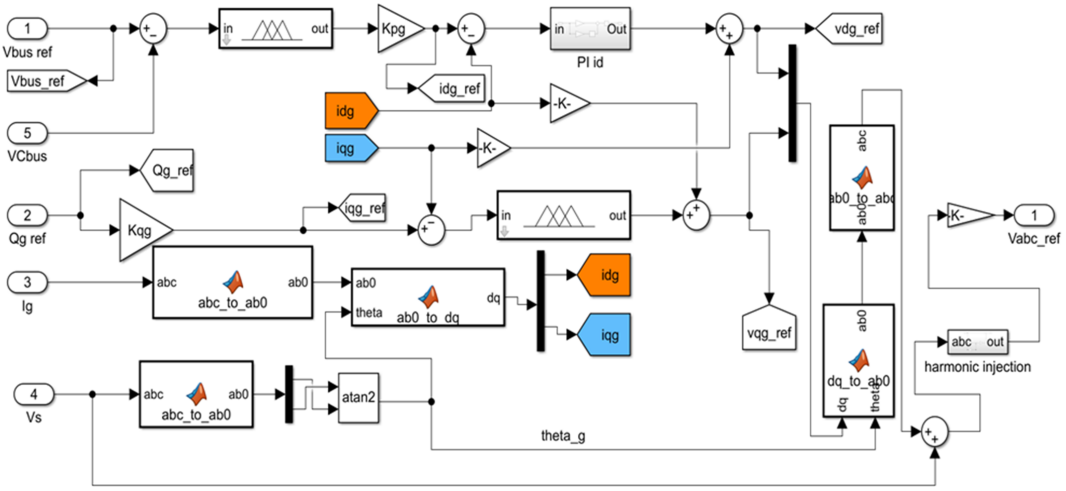

Figure 5. The GSC of the suggested method

7. Simulation results and discussions

To simulate the system decribed in Figure 3, the data of the WT based DFIG are given in Appendix A and it is taken from reference [9]. The fault event obeys the netwrok regulation described by Figure 1. Two scenarios are simulated, the fisrt by simulation of the system without the CB, and the second with the CB ciruit.

7.1 *Fault event description*

The machine is started from zero speed, till it reaches steady state, then a three phase voltage drop of 90% has been ocuured such that the SV is 0.1 pu of its normal value. The VD continued for 0.15 s, then the SV recovered in 0.1 s as shown in Figure 6.

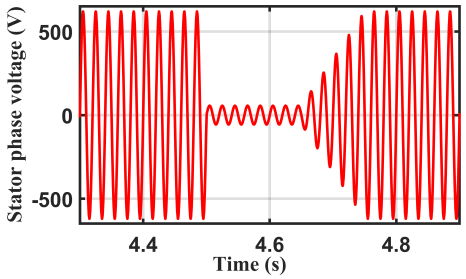

Figure 6. The SV with the symmetrical 3-phase voltage dip of 90%

7.2 *Operation without a CB circuit*

The simultion revealed, if the CB is not inserted to the system, the system variables, such as rotor velocity and currents becomes excessive and lead to systme instability. This emphasis on the importance of the existence of a CB circuit.

7.3 *Operation with a CB circuit*

If the CB is connected to the systems, the CB circuit senses the VD, it is activated, and its current is shown in Figure 7. The CB reaches more than 4,000 A at startig then it decays rabidly.

Both the SAR fluxes are shown in Figures 8 and 9. Both fiqures show the high transient component of the flux during the VD, and how the transient component affect on the shape of the flux.

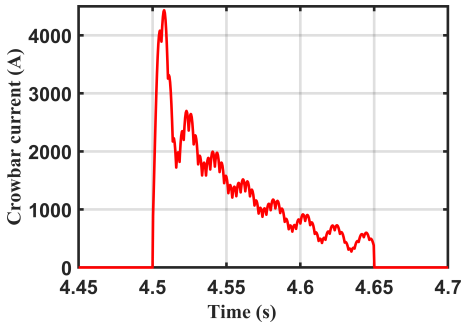

Figure 7. Variation of the CB current with time

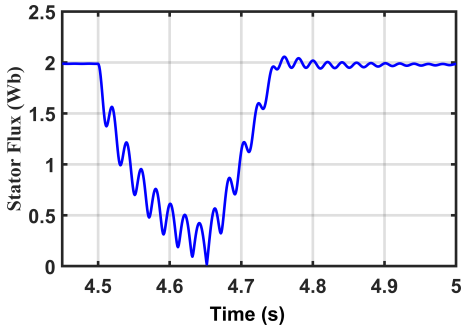

Figure 8. Varaiation of the SF with time

As seen from both Figures 8 and 9, there is a sharp fall in both stator field and rotor field during the VD. Both fluxes nearly reaches zero value due to the VD. But as the voltage is restored to its rated value, both fluxes re-established their nominal values. The machine electromagnetic torque is shown in Figure 10.

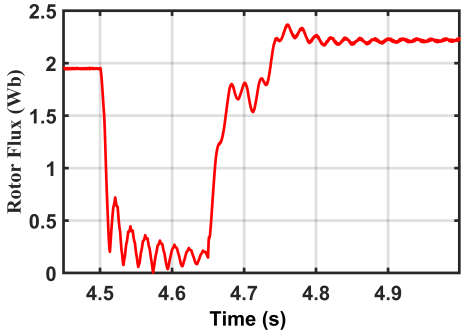

Figure 9. Shape of the rotor field

The torque is strongly affected by the VD as seen by sharp change in the torque value, and fluctautes around zero value, but the controller retrieves the torque to its steady state.

The rotor velocity in rpm is displayed in Figure 11. The velocity is raised during the VD due to the decrease in the electromagnetic torque, but the controller succeeded to regain the speed to its steady state.

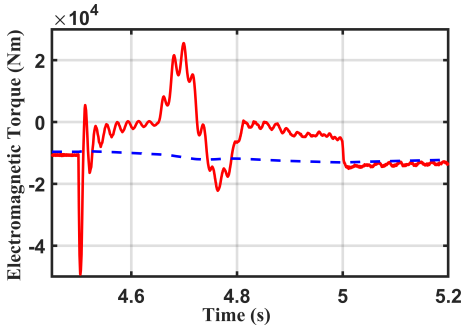

Figure 10. The DFIG electromagnetic torque variation with time

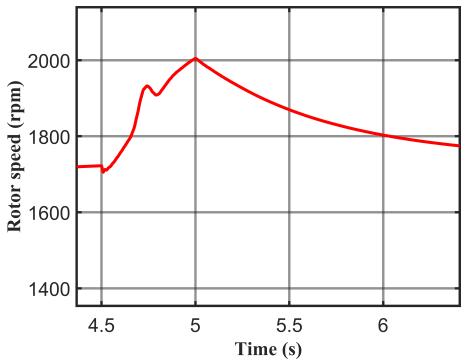

Figure 11. The rotor speed in rpm

The ROTCNT is presented in Figure 12. The ROTCNT has high increase during the VD, but the controller sucesseded to regain the current to its steady state. The rotor voltage displayed in Figure 13. It can be noticed that, before the VD, the RV has a voltage pulses resulted from the inverter and the at begeining of the VD, the CB is activated and isolated the rotor ciricut so that the RV has two compoenets transient and sinusoidal component as shown in Figure 13. There is an abrupt change in the rotor voltage due to the voltage dip, but it decays to zero, till the CB is deactivated and the RV attains its prefault value. Similar explanation can be noticed from the SC shown in Figure 14. The SC has a high abrupt increase during the VD, nearly reaches above 5,000 A, but the controller retains the speed to its steady state.

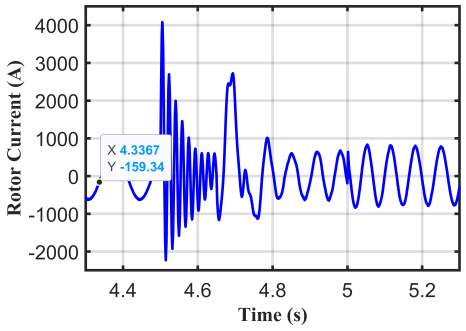

Figure 12. The time vataition of the ROTCNT

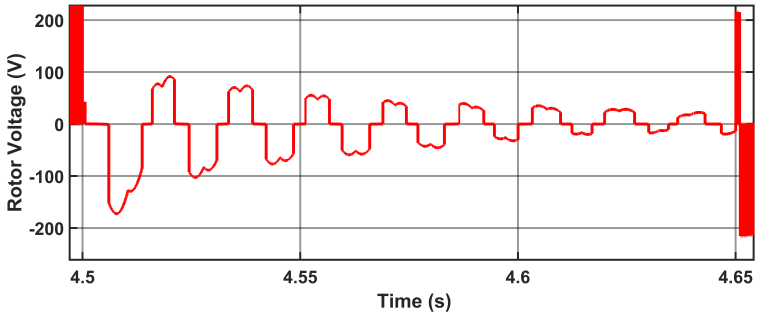

Figure 13. Rotor voltage response with time

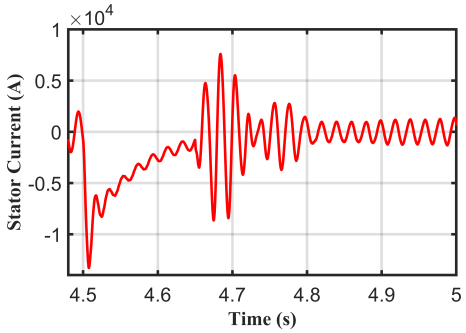

Figure 14. SC varaiation with time

The GSC variables are displayed in Figures 15 and 16. The voltage of the DCL is ilustrated in Figure 15, which indicates that, although the DCLV is enflunced by the VD, but it regains its steady state value. The grid current varaiation is shown in Figure 16 and it has a large over shoot at the beginning of the VD, but it regains its steady state value as shown from the Figure.

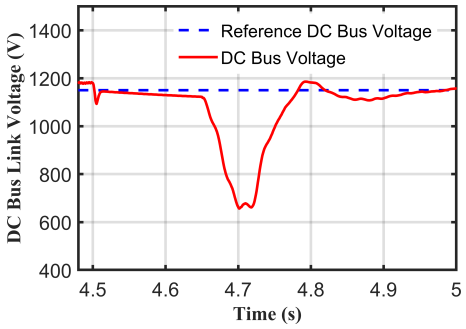

Figure 15. The DCL voltage response with time

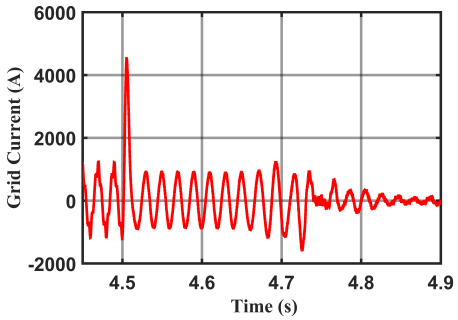

Figure 16. The grid current response with time

8. Conclusions

The DFIG is the best and suitable generator to be used in WT owing to it has a LVRT ability. With the help of proper control of the DFIG, it is possible to get high and efficient performance during both steady-state and transient conditions. Since power system is sustainable to voltage fluctuations, it is desire to boost the LVRT of the DFIG. The present work recommends a hybrid control scheme to cope with the LVRT issue. The first part of the hybrid scheme is to utilize of a CB circuit which is very efficient to handle with the stationary transient component of the voltage and current produced in the rotor circuit. Without this CB circuit, the system could be unstable for severe voltage dips. The other part of the hybrid schme, is to use both the RSC and GSC to regulate the machine to enhance the LVRT. The RSC is controlled such that it can inject reactive power while the GSC is controlled such that it keeps the DC voltage constant. An ANFIS controller has been suggested and the results show the validity of the proposed ANFIS technique to cope with any severe voltage fluctuations or disturbances. Simulation results showed the high performance of the suggested method, and the suggested control keeps the stability of the DFIG and settles the system in minimum time with high transient performance.

Appendix A: Used system data

Mechanical system data		
Parameter	Value	Unit
Low speed axle inertia $J_{t,a}$	800	Kg · m^2
Low speed axle friction $D_{t,a}$	0.1	Nm · s/rad
Coupling stiffness K_{tm}	12,500	Nm/rad
Coupling damping D_{tm}	130	Nm · s/rad
High speed axle inertia J_m	90	Kg · m^2
High speed axle friction D_m	0.1	Nm · s/rad
Data of the generator		
Parameter	Value	Unit
Rated stator active power P_s	2.0	MW
Nominal torque T_e	12,732	Nm
Stator voltage V_s	690	V
Nominal speed ω	1,500	rpm
Speed range	900-2,000	rpm
Pole pairs P	2	
Magnetizing inductance, L_m	2.5	mH
Rotor leakage inductance, $L_{\sigma r}$	87	μH
Stator leakage inductance, $L_{\sigma s}$	87	μH
Rotor resistance, R_r	0.026	Ω
Stator resistance, R_s	0.029	Ω

Data avaliability statement

The data that support the findings of this study are available from the corresponding author upon reasonable request.

Conflict of interest

The authors declare that they have no conflict of interest.

Ethics and consent to participate declarations

Not applicable.

Human and animal rights

This article does not contain any studies with animals performed by any of the authors.

References

[1] M. A. Mostafa, E. A. El-Hay, and M. M. Elkholy, "An overview and case study of recent low voltage ride through methods for wind energy conversion system," *Renewable and Sustainable Energy Reviews*, vol. 183, p. 113521, 2023.

[2] Z. Yang, B. Gao, and Z. Cao, "Low-voltage ride-through strategy for offshore wind turbines based on current relaxation region," *Electric Power Systems Research*, vol. 223, p. 109704, 2023.

[3] M. G. Marcelo and J. G. Alvarez, "Technical and regulatory exigencies for grid connection of wind generation," in *Wind Farm: Technical Regulations, Potential Estimation and Siting Assessment*, O. S. Gastón, Ed. Rijeka: IntechOpen, 2011, ch. 1.

[4] I. Erlich and U. Bachmann, "Grid code requirements concerning connection and operation of wind turbines in Germany," in *Proc. IEEE Power Engineering Society General Meeting*, San Francisco, CA, USA, Jun. 12-16, 2005.

[5] A. M. Moheb, E. A. El-Hay, and A. A. El-Fergany, "Comprehensive review on fault ride-through requirements of renewable hybrid microgrids," *Energies*, vol. 15, no. 18, p. 6785, 2022.

[6] D. Grid Code, *Grid Code*, 2005.

[7] J. Joshi, A. K. Swami, V. Jately, B. Azzopardi, "A comprehensive review of control strategies to overcome challenges during LVRT in PV systems," *IEEE Access*, vol. 9, pp. 121804-121834, 2021.

[8] A. M. Moheb, E. A. El-Hay, and A. A. El-Fergany, "Consolidation of LVFRT capabilities of microgrids using energy storage devices," *Scientific Reports*, vol. 13, no. 1, p. 22294, 2023.

[9] G. Abad, J. Lopez, M. Rodriguez, L. Marroyo, G. Iwanski, *Doubly Fed Induction Machine: Modeling and Control for Wind Energy Generation*. Hoboken, NJ, USA: Wiley, 2011.

[10] B. Aljafari, J. Pamela Stephenraj, I. Vairavasundaram, R. Singh Rassiah, "Steady state modeling and performance analysis of a wind turbine-based doubly fed induction generator system with rotor control," *Energies*, vol. 15, no. 9, p. 3327, 2022.

[11] R. A. Oliveira and M. H. Bollen, "Magnification of transients at the voltage dips starting and its impacts on DFIG-based wind power plants," *Electric Power Systems Research*, vol. 211, p. 108244, 2022.

[12] J. Tait, S. Wang, K. Ahmed, G. P. Adam, "Comparative assessment of four low voltage fault ride through techniques (LVFRT) for wind energy conversion systems (WECSs)," *Alexandria Engineering Journal*, vol. 61, no. 12, pp. 10463-10476, 2022.

[13] O. Gomis-Bellmunt, A. Junyent-Ferre, A. Sumper, J. Bergas-Jane, "Ride-through control of a doubly fed induction generator under unbalanced voltage sags," *IEEE Transactions on Energy Conversion*, vol. 23, no. 4, pp. 1036-1045, 2008.

[14] M. Nasiri, J. Milimonfared, and S. H. Fathi, "A review of low-voltage ride-through enhancement methods for permanent magnet synchronous generator based wind turbines," *Renewable and Sustainable Energy Reviews*, vol. 47, pp. 399-414, 2015.
[15] M. Tsili and S. Papathanassiou, "A review of grid code technical requirements for wind farms," *IET Renewable Power Generation*, vol. 3, no. 3, pp. 308-332, 2009.
[16] A. K. Thet and H. Saitoh, "Pitch control for improving the low-voltage ride-through of wind farm," in *Proc. 2009 Transmission & Distribution Conference & Exposition: Asia and Pacific*, Seoul, South Korea, Oct. 26-30, 2009.
[17] J.-h. Zhu, P. Zhang, X. Zhang, L. Qin, C. Sun, H. Li, "Model predictive control on transient flux linkage and reactive power compensation of doubly fed induction wind generator," *International Journal of Energy Research*, vol. 2024, p. 6648691, 2024.
[18] A. Achar, Y. Djeriri, H. Benbouhenni, R. Bouddou, Z. M. S. Elbarbary, "Modified vector-controlled DFIG wind energy system using robust model predictive rotor current control," *Arabian Journal for Science and Engineering*, 2024. https://doi.org/10.1007/s13369-024-09310-0.
[19] K. Gayathri and S. Jeevananthan, "Refined vector control structure and indirect MPPT for grid connected DFIG-based wind energy conversion system, and appraisal on matrix converter interface," *International Journal of Modelling, Identification and Control*, vol. 44, no. 3, pp. 255-282, 2024.
[20] Y. Moumani, A. J. Laafou, A. Ait Madi, R. Boutssaid, "An improved dual vector control for a doubly fed induction generator based wind turbine during asymmetrical voltage dips," *Bulletin of Electrical Engineering and Informatics*, vol. 13, no. 5, pp. 3757-3769, 2024.
[21] B. Qin, H. Li, X. Zhou, J. Li, W. Liu, "Low-voltage ride-through techniques in DFIG-based wind turbines: A review," *Applied Sciences*, vol. 10, no. 6, p. 2154, 2020.
[22] O. P. Mahela, N. Gupta, M. Khosravy, N. Patel, "Comprehensive overview of low voltage ride through methods of grid integrated wind generator," *IEEE Access*, vol. 7, pp. 99299-99326, 2019.
[23] Y. Han, Y. Feng, P. Yang, L. Xu, Y. Xu, F. Blaabjerg, "Cause, classification of voltage sag, and voltage sag emulators and applications: A comprehensive overview," *IEEE Access*, vol. 8, pp. 1922-1934, 2020.
[24] H. Ghaffarzadeh and A. Mehrizi-Sani, "Review of control techniques for wind energy systems," *Energies*, vol. 13, no. 24, p. 6664, 2020.
[25] L. Li, Y. Liang, J. Niu, J. He, H. Liu, B. Li, C. Li, Y. Cao, "The fault ride-through characteristics of a double-fed induction generator using a dynamic voltage restorer with superconducting magnetic energy storage," *Applied Sciences*, vol. 13, no. 14, p. 8180, 2023.
[26] A. H. K. Alaboudy, H. A. Mahmoud, A. A. Elbasetm, M. Abdelsattar, "Technical assessment of the key LVRT techniques for grid-connected DFIG wind turbines," *Arabian Journal for Science and Engineering*, vol. 48, pp. 15223-15239, 2023.
[27] S. M. Endale and M. B. Tuka, "Fault ride through capability analysis of wind turbine with doubly fed induction generator," *Preprints*, 2021. https://doi.org/10.20944/preprints202107.0476.v1.
[28] M. H. Haque, "Compensation of distribution system voltage sag by DVR and D-STATCOM," in *Proc. 2001 IEEE Porto Power Tech Conference*, Porto, Portugal, Sep. 10-13, 2001, vol. 1, pp. 5-9.
[29] R. Uthra and D. Suchitra, "A fuzzy based improved control strategy of dynamic voltage restorer for low voltage and high voltage ride through compensation for variable speed hybrid energy system," *Wireless Personal Communications*, vol. 127, no. 3, pp. 2391-2415, 2022.
[30] W. S. Hassanein, M. M. Ahmed, M. O. abed el-Raouf, M. G. Ashmawy, M. I. Mosaad, "Performance improvement of off-grid hybrid renewable energy system using dynamic voltage restorer," *Alexandria Engineering Journal*, vol. 59, no. 3, pp. 1567-1581, 2020.
[31] P. M. Ingle and V. S. Chavhan, "Improving the LVRT capability of the DFIG-based wind turbines during fault," *International Journal for Multidisciplinary Research*, vol. 5, no. 1, pp. 1-5, 2023.
[32] H. Rezaie and M. H. Kazemi-Rahbar, "Enhancing voltage stability and LVRT capability of a wind-integrated power system using a fuzzy-based SVC," *Engineering Science and Technology, an International Journal*, vol. 22, no. 3, pp. 827-839, 2019.
[33] R. R. Hete, S. K. Mishra, R. Dash, A. Ballaji, V. Subburaj, K. J. Reddy, "Analysis of DFIG-STATCOM P2P control action using simulated annealing techniques," *Heliyon*, vol. 8, no. 3, p. e09125, 2022.
[34] I. N. Muisyo, C. M. Muriithi, and S. I. Kamau, "Enhancing low voltage ride through capability of grid connected DFIG based WECS using WCA-PSO tuned STATCOM controller," *Heliyon*, vol. 8, no. 8, p. e10042, 2022.

[35] C. Ding, H. You, and Y. Guo, "Low voltage ride through of doubly-fed wind farm based on STATCOM with fuzzy PI control," in *Proc. 2023 6th International Conference on Energy, Electrical and Power Engineering*, Chongqing, China, May 12-14, 2023.

[36] S. K. Samal, R. T. Shivaji, and S. Karad, "STATCOM with fuzzy-PI controller for low voltage-ride through enhancement of DFIG based wind farm," *International Journal of Emerging Trends in Engineering Research*, vol. 9, no. 12, pp. 132-140, 2021.

[37] K. Lella and R. M. Mohan, "Application of bridge type fault current limiter for fault ride-through capability enhancement of DFIG based variable speed wind turbines," *Engineering, Environmental Science*, vol. 17, no. 2, p. 8, 2020.

[38] S. Saeed, R. Asghar, F. Mehmood, H. Saleem, B. Azeem, Z. Ullah, "Evaluating a hybrid circuit topology for fault-ride through in DFIG-based wind turbines," *Sensors*, vol. 22, no. 23, p. 9314, 2022.

[39] N. M. Khoa, D. D. Tung, and L. V. Dai, "Experimental study on low voltage ride-through of DFIG-based wind turbine," *International Journal of Electrical and Electronic Engineering & Telecommunications*, vol. 11, no. 1, pp. 1-11, 2022.

[40] P. Makolo, J. J. Justo, F. Mwasilu, R. Zamora, "Fault ride through technique for DFIG-based wind turbines under grid three-phase faults," in *Proc. 2018 Australasian Universities Power Engineering Conference*, Auckland, New Zealand, Nov. 27-30, 2018.

[41] T. Joshiram and S. V. R. L. Kumari, "Power quality enhancement and low voltage ride through capability in hybrid grid interconnected system by using D-FACT devices," in *Emerging Technologies for Computing, Communication and Smart Cities*, Singapore: Springer, 2022, pp. 215-230.

[42] D. Vilathgamuwa, C. J. Gajanayake, P. C. Loh, Y. W. Li, "Voltage sag compensation with Z-source inverter based dynamic voltage restorer," *IEEE Transactions on Power Electronics*, vol. 21, no. 5, pp. 2242-2248, 2006.

[43] A. Komijani, M. Sedighizadeh, and M. Kheradmandi, "Improving fault ride-through in meshed microgrids with wind and PV by virtual synchronous generator with SFCL and SMES," *Journal of Energy Storage*, vol. 50, p. 103952, 2022.

[44] J. Yin, "Influence of reactive power support control strategy on short-circuit current calculation and fault analysis method of DFIG," *Energy Reports*, vol. 7, pp. 5933-5942, 2021.

[45] J. Gu, Z. Zhang, Z. Li, J. Rodriguez, "Model predictive control for DFIG to improve the LVRT capability under severe asymmetrical grid faults," in *Proc. 2023 IEEE International Conference on Predictive Control of Electrical Drives and Power Electronics*, Wuhan, China, Jun. 16-18, 2023.

[46] V. Yaramasu, B. Wu, S. Alepuz, S. Kouro, "Predictive control for low-voltage ride-through enhancement of three-level-boost and NPC-converter-based PMSG wind turbine," *IEEE Transactions on Industrial Electronics*, vol. 61, no. 12, pp. 6832-6843, 2014.

[47] M. Soliman, O. P. Malik, and D. T. Westwick, "Ensuring fault ride through for wind turbines with doubly fed induction generator: A model predictive control approach," *IFAC Proceedings Volumes*, vol. 44, no. 1, pp. 1710-1715, 2011.

[48] B. Kumar, K. S. Sandhu, and R. Sharma, "Comparative analysis of control schemes for DFIG-based wind energy system," *Journal of The Institution of Engineers (India): Series B*, 2021.

[49] A. Vardhan and R. Saxena, "Vector control of DFIG-based wind turbine system," *International Journal of Electrical Engineering & Technology*, vol. 16, no. 3, pp. 348-358, 2022.

[50] H. Yuan, D. Wang, and X. Zhou, "Frequency support of DFIG-based wind turbine via virtual synchronous control of inner voltage vector," *Electric Power Systems Research*, vol. 225, p. 109823, 2023.

[51] M. Chowdhury, G. Shafiullah, and S. Ferdous, "Low voltage ride-through augmentation of DFIG wind turbines by simultaneous control of back-to-back converter using partial feedback linearization technique," *International Journal of Electrical Power & Energy Systems*, vol. 153, p. 109394, 2023.

[52] M. A. Mostafa, E. A. El-Hay, and M. M. Elkholy, "Optimal low voltage ride through of wind turbine doubly fed induction generator based on bonobo optimization algorithm," *Scientific Reports*, vol. 13, no. 1, p. 7778, 2023.

[53] M. Soomro, Z. A. Memon, M. H. Baloch, N. H. Mirjat, L. Kumar, Q. T. Tran, G. Zizzo, "Performance improvement of grid-integrated doubly fed induction generator under asymmetrical and symmetrical faults," *Energies*, vol. 16, no. 8, p. 3350, 2023.

[54] A. H. K. Alaboudy, A. A. Elbaset, and M. Abdelsattar, "A case study on the LVRT capability of an Egyptian electrical grid linked to the Al-Zafarana wind park using series resistor," *International Journal of Renewable Energy Research*, vol. 13, no. 1, pp. 36-48, 2023.

[55] R. Hiremath and T. Moger, "Improving the DC-link voltage of DFIG driven wind system using modified sliding mode control," *Distributed Generation & Alternative Energy Journal*, vol. 38, no. 3, pp. 715-742, 2023.
[56] M. S. H. Khan and S. K. Mallik, "R-SFCL and RRCOCS-TVC based cooperative control for enhancing LVRT capability of DFIG system," *Trends in Sciences*, vol. 19, no. 18, p. 5823, 2022.
[57] S. R. Mosayyebi, S. H. Shahalami, and H. Mojallali, "Fault ride-through capability improvement in a DFIG-based wind turbine using modified ADRC," *Protection and Control of Modern Power Systems*, vol. 7, no. 1, p. 50, 2022.
[58] Z. Rafiee, R. Heydari, M. Rafiee, M. R. Aghamohammadi, F. Blaabjerg, "Enhancement of the LVRT capability for DFIG-based wind farms based on short-circuit capacity," *IEEE Systems Journal*, vol. 16, no. 2, pp. 3237-3248, 2022.
[59] F. Herzog, J. Röder, A. Frehn, N. Ruhe, R. W. De Doncker, "Influences on the LVRT behavior of DFIG wind turbine systems," in *Journal of Physics: Conference Series*, vol. 2265, no. 3, p. 032007, 2022.
[60] J. Hu, Y. He, L. Xu, "Improved rotor current control of wind turbine driven doubly fed induction generators during network unbalance," in *Proc. 2009 International Conference on Sustainable Power Generation and Supply*, Nanjing, China, Apr. 6-7, 2009.
[61] M. Wang, W. Xu, and X. Yu, "A novel method to optimize the active crowbar resistance for low voltage ride through operation of doubly-fed induction generator based on wind energy," *IEEE Transactions on Energy Conversion*, vol. 27, no. 4, pp. 872-881, 2012.
[62] R. A. J. Amalorpavaraj, K. Palanisamy, S. Umashankar A. D. Thirumoorthy, "Power quality improvement of grid connected wind farms through voltage restoration using dynamic voltage restorer," *International Journal of Renewable Energy Research*, vol. 6, no. 1, pp. 53-60, 2016.
[63] S. K. Sahu, B. Y. Shivaji, and E. Borkar, "Analysis of fault ride through capability in DFIG based wind turbines using dynamic voltage restorer with PWM technique," *International Journal For Technological Research In Engineering*, vol. 8, no. 4, pp. 1-8, 2020.
[64] Y. Wang, Q. Wu, H. Xu, Q. Guo, H. Sun, "Fast coordinated control of DFIG wind turbine generators for low and high voltage ride-through," *Energies*, vol. 7, no. 7, pp. 4140-4156, 2014.
[65] J. R. Mohanty, B. B. Verma, P. K. Ray, D. R. K. Parhi, "Application of adaptive neuro-fuzzy inference system in modeling fatigue life under interspersed mixed-mode (I and II) spike overload," *Expert Systems with Applications*, vol. 38, no. 10, pp. 12302-12311, 2011.
[66] A. Nik-Khorasani, H. Sadoghi-Yazdi, and A. Mehrizi, "Robust hybrid learning approach for adaptive neuro-fuzzy inference systems," *Fuzzy Sets and Systems*, vol. 481, p. 108890, 2024.